# Neutron and PIMC Determination of the Longitudinal Momentum Distribution of HCP, BCC and Normal Liquid <sup>4</sup>He<sup>†,\*</sup>

R. C. Blasdell 1

Materials Science Division, Argonne National Laboratory, USA

D. M. Ceperley

Physics Department, University of Illinois at Urbana-Champaign, USA

R. O. Simmons

Physics Department and Materials Research Laboratory, University of Illinois at Urbana-Champaign, USA

Z. Naturforsch. 48 a, 433-437 (1993); received December 27, 1991

Deep inelastic neutron scattering has been used to measure the neutron Compton profile (NCP) of a series of condensed <sup>4</sup>He samples at densities from 28.8 atoms/nm<sup>3</sup> (essentially the minimum possible density in the solid phase) up to 39.8 atoms/nm<sup>3</sup> using a chopper spectrometer at the Argonne National Laboratory Intense Pulsed Neutron Source. At the lowest density, the NCP was measured along an isochore through the hcp, bcc, and normal liquid phases. Average atomic kinetic energies are extracted from each of the data sets and are compared to both published and new path integral Monte-Carlo (PIMC) calculations as well as other theoretical predictions. In this preliminary analysis of the data, account is taken of the effects of instrumental resolution, multiple scattering, and final-state interactions. Both our measurements and the PIMC theory show that there are only small differences in the kinetic energy and longitudinal momentum distribution of isochoric helium samples, regardless of their phase or crystal structure.

Key words: Momentum distribution; Neutron; Helium.

#### I. Introduction

Of great interest are the various quantum liquids and solids formed by condensing helium [1]. The atomic momentum distributions n(p) of these systems can now be probed directly, using deep inelastic neutron scattering (DINS) [2, 3]. Because the interatomic forces are well known [4], these quantum systems can also be studied by sophisticated computer simulations [5, 6]. Comparisons are then possible between essentially direct measurements of n(p) and essentially a priori calculations. The present work compares the results of recent DINS measurements on <sup>4</sup>He against

the predictions of several of these theoretical calculations.

At high momentum transfer  $\hbar Q$ , the scattering of neutrons from the nuclei in a condensed helium sample becomes incoherent and approaches the impulse-approximation limit of free-atom scattering, Doppler broadened by the distribution of initial <sup>4</sup>He atom velocities. In this limit the dynamic structure factor S(Q, E) scales [7] and it is convenient to convert the data to the neutron Compton profile J(y, Q) [8]

$$J(y,Q) = \frac{\hbar^2 Q}{M} S(Q, E), \qquad (1)$$

where M is the mass of a helium atom, and y is the vectorial West y-scaling variable

$$y = \frac{M}{\hbar^2 Q} \left( E - \frac{\hbar^2 Q^2}{2M} \right) \hat{Q}, \qquad (2)$$

which measures the scaled energy broadening of the scattering relative to the energy transfer for a stationary free atom. (E is the energy transferred to the helium atom in the scattering event.)

Reprint requests to Prof. R. O. Simmons, Physics Department, University of Illinois, 1110 W. Green St., Urbana, IL 61801, USA.

0932-0784 / 93 / 0100-0433 \$ 01.30/0. - Please order a reprint rather than making your own copy.

<sup>†</sup> Supported by the U.S. Department of Energy, BES-Materials Sciences under Contract Nos. DEFG02-91ER45439 and W-31-109-ENG-38.

Permanent address: Physics Department, University of Illinois at Urbana-Champaign, USA.

<sup>\*</sup> Presented at the Sagamore X Conference on Charge, Spin and Momentum Densities, Konstanz, Fed. Rep. of Germany, September 1-7, 1991.

As Q approaches infinity, J(y, Q) approaches  $n_{\parallel}(y)$ , the longitudinal momentum distribution, which is the probability density that an atom will have component of momentum  $\hbar y$  along the  $\hat{Q}$  direction. For a system with an isotropic n(p), and for z along the  $\hat{Q}$  direction,

$$n_{\parallel}(p_z) = \iint \mathrm{d}p_x \, \mathrm{d}p_y \, n(\mathbf{p}) \,. \tag{3}$$

Any differences between J(y, Q) and  $n_{\parallel}(y)$  are attributed to final-state effects (FSE). The present data were taken at an average momentum transfer of 235 nm<sup>-1</sup>, which is sufficiently high to make FSE corrections to  $n_{\parallel}(y)$  small but not negligible.

Green's Function Monte-Carlo (GFMC) calculations suggest that n(p) is isotropic in solid <sup>4</sup>He [6]. This is assumed throughout the present work. Because the present experimental measurements and theoretical calculations both represent spherical averages of J(y, Q) and  $n_{\parallel}(y)$ , respectively, over crystallographic orientations, this should not prevent a precise comparison of theory and experiment even if there is a small amount of anisotropy in n(p).

## II. Experiment

DINS data sets have been taken on solid and normal liquid <sup>4</sup>He at densities ranging from 28.80 atoms/ nm<sup>3</sup> to 39.81 atoms/nm<sup>3</sup> and at temperatures ranging from 0.55 K to 5.75 K. At the lowest density, the NCP was measured along an isochore through the hcp solid, bcc solid, and normal liquid. Table 1 shows the density and temperature for each of the samples reported here. All of the present measurements were taken with the Phoenix neutron time-of-flight chopper spectrometer at the Intense Pulsed Neutron Source at Argonne National Laboratory. The samples were grown in one of two pressure cells. The first cell consists of seven vertical tubes arranged in a plane at 45° to the incident neutron beam. The second cell is essentially the same but with six tubes. Each of the solids was characterized by removing the neutron choppers and using the spectrometer as a diffractometer. The cited densities are obtained from fits to the diffraction data using a standard silicon sample for calibration. The diffraction data, as well as thermometry and pressure measurements, show conclusively that the bcc sample was in fact entirely within the narrow bcc portion of the 4He phase diagram. In general each sample tube contained at least several crystallites so that the observed scattering from the set of six (or

Table 1. Average atomic kinetic energies,  $\langle E_{\bf k} \rangle$ , of solid and normal liquid <sup>4</sup>He.

Expt. or theory	Phase	T/K	Density $\varrho/\text{atoms nm}^{-3} \langle E_k \rangle/K$	
Expt.	hcp	1.070	28.80	23.6
Expt.	bcc	1.725	28.80	23.7
Expt.	liquid	2.705	28.80	24.2
PIMC a	fcc	1.600	28.82	24.4
PIMC a	bcc	1.667	28.82	24.1
PIMC a	liquid	2.353	28.82	24.8
PIMC a	liquid	4.000	28.82	25.7
SCP b	bcc	_	28.74	19.5
Expt.	hcp	1.48	29.64	25.2
PIMC	hcp	1.482	29.64	25.6
GFMC c	fcc	0	29.4	25.7
GFMC c	fcc	0	31.5	28.3
GFMC c	fcc	0	33.5	31.8
Expt.	hcp	1.44	34.59	34.1
PIMC	hcp	1.43	34.61	33.2
GFMC c	fcc	0	35.3	33.3
Expt.	hcp	1.507	39.81	43.9
Expt.	hcp	5.75	39.81	44.0
PIMC	hcp	5.71	39.80	42.7

<sup>&</sup>lt;sup>a</sup> Ref. [10]. - <sup>b</sup> Ref. [9]. - <sup>c</sup> Ref. [6].

seven) sample cylinders represents a reasonable average of the NCP over crystallographic orientations.

Two DINS time-of-flight neutron spectra were taken for each sample: one with helium in the aluminum pressure cell and one with the cell empty. The difference of the two spectra is converted to J(y, Q), and an estimate of the multiple scattering, as calculated by a comprehensive Monte-Carlo simulation of the instrument response, is subtracted from the data.

The instrument Monte-Carlo simulation is also used to determine the effective instrumental resolution function in J(y, Q). The simulation takes account of the finite neutron source moderator geometry, the full moderator neutron emission distribution, the actual geometry of the chopper absorbing slats, the finite sample geometry, the multiple scattering in the sample and pressure cell, the attenuation of the incident and scattered neutron beams in the sample and pressure cell, and the multiple scattering in the walls of the detectors and beam monitors.

#### III. Results and Analysis

Figure 1 compares the measured neutron Compton profiles J(y, Q) (corrected for multiple scattering) for the bcc solid, hcp solid, and normal liquid at a constant density of 28.80 atoms/nm<sup>3</sup>. There are no

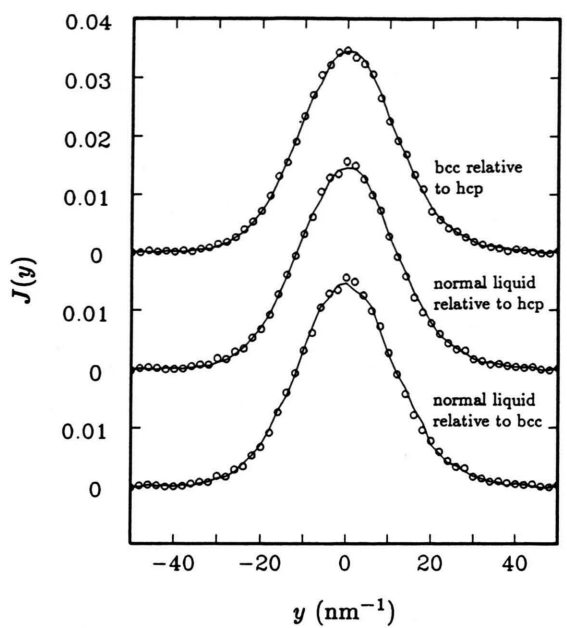


Fig. 1. Measured neutron Compton profiles J(y) for the bcc solid, hcp solid, and normal liquid corrected for multiple scattering at a constant density of 28.80 atoms/nm³ and an average Q of 235 nm $^{-1}$ . The top curves compare the bcc (circles) and hcp (solid) data, the middle curves compare the normal liquid (circles) and hcp (solid) data, and the bottom curves compare the normal liquid (circles) and bcc (solid) data. We observe no significant difference in the shape or second moment  $(\langle E_k \rangle)$  of J(y) even though the samples are at different temperatures, at different pressures, and possess different spatial ordering.

obvious systematic differences in either the widths or shapes of the Compton profiles even though the samples are at different temperatures, at different pressures, and possess different spatial ordering.

The data are fitted assuming an isotropic Gaussian longitudinal momentum distribution  $n_{\parallel}(y)$  with the neutron Compton profile expressed as the leading three terms in the Sears expansion [8]:

$$J(y, Q) = n_{\parallel}(y) + j_{3}(Q) \frac{\partial^{3} n_{\parallel}(y)}{\partial^{3} y} + j_{4}(Q) \frac{\partial^{4} n_{\parallel}(y)}{\partial^{4} y}.$$
 (4)

The model form of J(y, Q) is convolved with the effective instrumental resolution function and fitted to the data in J(y) with a  $\chi^2$  fitting routine assuming that Q is constant in the measurements. (In reality, Q changes by about  $\pm 10\%$  across the peak in the observed scattering.) The results of a fit to the bcc solid is shown in Figure 2. The fits are all statistically plausible (v is the number of degrees of freedom, and  $\chi^2$  the

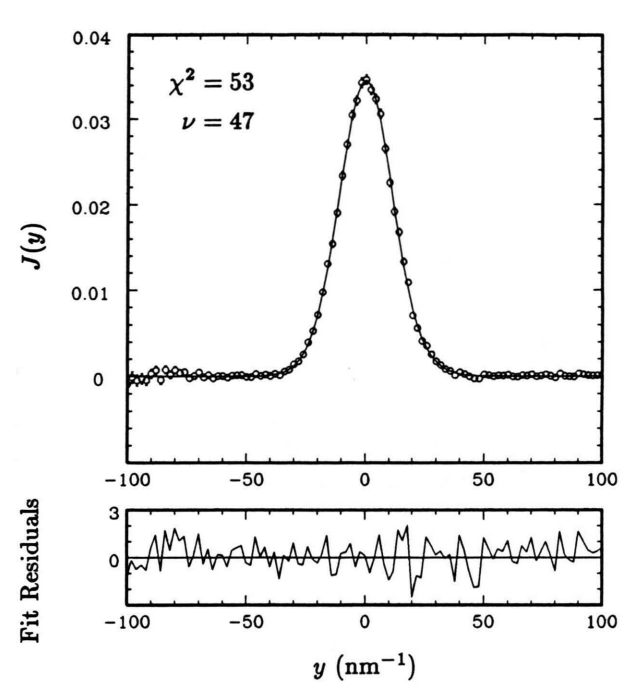


Fig. 2. Fit of a Gaussian  $n_{\parallel}(y)$  with Sears FSE corrections (solid) to the bcc solid neutron Compton profile J(y,Q) corrected for multiple scattering (circles). An effective instrumental resolution function determined by Monte-Carlo simulation is convolved with the model form (4) of J(y). The fit residuals ([data—fit]/uncertainty of data) are shown at the bottom. In contrast to earlier high-Q measurements, all of the fits are statistically plausible (v is the number of degrees of freedom, and  $\chi^2$  is the unreduced chi-squared of the fit).

unreduced chi-squared of the fit), and show no obvious residual systematic backgrounds.

Figure 3 shows the relative peak amplitude of the fitted Sears FSE correction factors  $j_3$  and  $j_4$  compared to the peak amplitude of  $n_{\parallel}(y)$  as a function of density. The Sears expansion provides a consistent description of the data. Ignoring these corrections increases  $\chi^2$  significantly. It is interesting that the relative amplitude of the symmetric  $j_4$  term appears to grow at low densities. At this time we do not believe that any significant information on higher-order terms in the expansion can be extracted from the data.

Figure 4 compares the theoretical predictions of the average atomic kinetic energies  $\langle E_{\mathbf{k}} \rangle$  (proportional to the second moment of J(y)) to the values extracted from the fits to the experimental data. Several of the points overlap significantly, and so the plotted values are also given in Table 1. At these low temperatures,  $\langle E_{\mathbf{k}} \rangle$  is dominated by the quantum zero-point effect. Both theory and experiment find that  $\langle E_{\mathbf{k}} \rangle$  depends

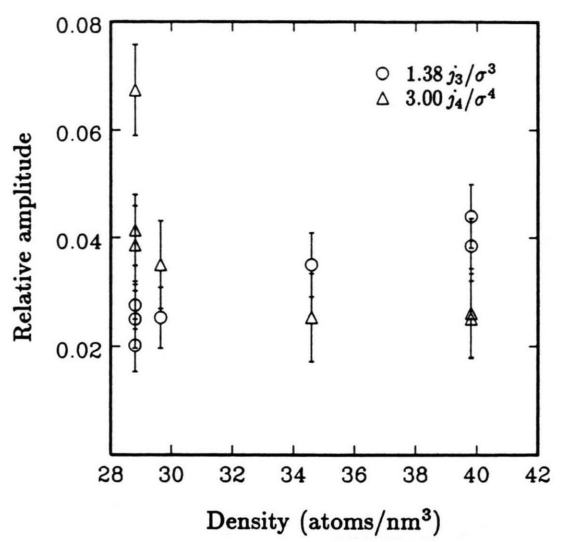


Fig. 3. Relative peak amplitudes of the Sears FSE corrections to the impulse approximation as determined by fits to the data.  $j_3$  is the amplitude of the first antisymmetric correction and  $j_4$  is the amplitude of the first symmetric correction. The smooth variation of the amplitude of the Sears FSE corrections with density, as well as the substantial improvement of  $\chi^2$  upon inclusion of the Sears corrections in the fits suggests that they are a valid way of correcting for FSE's in the solid and normal liquid.

strongly upon the density of the condensed helium, but depends little on the nature of the condensed phase at constant density, whether hcp or bcc solid, or indeed normal liquid. PIMC finds a small temperature dependence of  $\langle E_{\bf k} \rangle$  at the lowest density. The experimental data show no temperature dependence in  $\langle E_{\bf k} \rangle$  above the statistical uncertainty of about  $\pm 0.3$  K.

Both the GFMC and PIMC calculations have used the Aziz HFDHE2 potential [4]. Given the relatively good agreement of these theories with the experimental measurements of  $\langle E_k \rangle$ , we conclude that this potential provides a reasonable description of the dynamics of condensed helium up to the density of 40 atom/nm<sup>3</sup>.

The self-consistent phonon (SCP) calculation [9] is significantly ( $\sim 20\%$ ) lower than experiment as well as the other two theoretical calculations. Both the PIMC and GFMC calculations are on the order of 2% lower than experiment at the higher densities. We are currently studying the systematic uncertainties in the re-

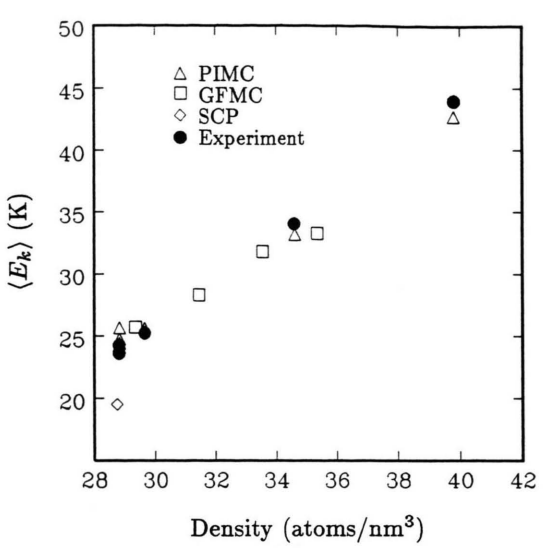


Fig. 4. Average kinetic energies  $\langle E_k \rangle$  for solid and normal liquid <sup>4</sup>He. The triangles are the PIMC results, the squares are the GFMC results, the diamond is the self-consistent phonon (SCP) result, and the solid circles are the experimentally determined  $\langle E_k \rangle$ . The statistical uncertainties of the experimental values are less than the size of the points. The systematic uncertainties are currently being examined.

duction of the data to decide if these differences are significant. In particular, we believe that the highestdensity experimental point may be somewhat too high.

Final-State Effect corrections are significant in the condensed helium phases even at these high momentum transfers. The Sears expansion for J(y) in terms of  $n_{\parallel}(y)$  describes these corrections well. Our measurements now have sufficient precision to examine longitudinal momentum distributions  $n_{\parallel}(y)$  directly, not just to measure average quantities such as  $\langle E_{\bf k} \rangle$ . Such detailed analyses, as well as an examination of the size of the systematic uncertainties in the  $\langle E_{\bf k} \rangle$ ,  $j_3$ , and  $j_4$ -measurements are underway.

## Acknowledgement

This research has benefited from the use of the Intense Pulsed Neutron Source (IPNS) at Argonne National Laboratory. This facility is funded by the U.S. Department of Energy, BES-Materials Sciences.

- [1] Can. J. Phys. 65, issue No. 11 (Nov. 1987, Proceedings of the Banff Conference on Quantum Fluids and Solids).
  [2] P. C. Hohenberg and P. L. Platzman, Phys. Rev. 152,
- 198 (1966).
- [3] R. O. Simmons, Can. J. Phys. 65, 1401 (1987). R. O. Hilleke, P. Chaddah, R. O. Simmons, D. L. Price, and
- S. K. Sinha, Phys. Rev. Lett. 52, 847 (1984).

  [4] R. A. Aziz, V. P. S. Nain, J. S. Carley, W. L. Taylor, and G. T. McConville, J. Chem. Phys. 70, 4330 (1979).

  R. A. Aziz, in: Inert Gases, Chapter 2 (M. L. Klein, ed.), Springer-Verlag, New York 1984.
- [5] D. M. Ceperley and E. L. Pollock, Can. J. Phys. 65, 1416 (1987)
- [6] P. Whitlock and R. M. Panoff, Can. J. Phys. 65, 1409

- (1987).
  [7] G. B. West, Phys. Rep. 18 C, 264 (1975).
  [8] V. F. Sears, Phys. Rev. B 30, 44 (1984).
  [9] L. K. Moleko and H. R. Glyde, Phys. Rev. Lett. 54, 901
- [10] D. Ceperley, in: Momentum Distributions, p. 71 (R. N. Silver and P. E. Sokol, eds.), Plenum Press, New York 1989.